FLOW OF WATER-BASED Cu, CuO, AND Al_2O_3 NANOFLUIDS HEATED WITH CONSTANT HEAT FLUX BETWEEN MICROPIPE

by

Hatice SIMSEK *

Tekirdag Namik Kemal University, Vocational School of Technical Sciences, Tekirdag, Turkey

Original scientific paper
https://doi.org/10.2298/TSCI2204941S

This study aims to analytically measure the fully developed laminar flow and heat transfer the water-based nanofluids, Cu, CuO, and Al_2O_3, within a micropipe with constant heat flux, under the temperature jump and slip rate boundary conditions. Knudsen number, nanoparticle volumes, and ratios of liquid layer thickness to particle radius are assumed, 0, 0.02, 0.04; 0%, 4%, %8, and 0.1, 0.2, 0.4, respectively. The findings suggest that adding nanoparticles to flow area has significant effect on both the velocity field and the heat transfer. There is a significant decline in the velocity both at the core and on the walls in the velocity area, due to the increase in the solid volume and the ratios of liquid layer thickness to particle radius after adding nanoparticles to flow area, and the increase of Nusselt number is significantly proportional to that of the solid volume and the ratios of liquid layer thickness to particle radius. Among the nanoparticles, Cu, CuO, and Al_2O_3, used as nanofluids within the micropipe, Cu is found to be the one with the highest heat transfer enhancement, followed by Al_2O_3, and CuO, respectively.

Key words*: micropipe, nanofluid, water, Cu, CuO, Al_2O_3, slip flow, slip factor, Nusselt number*

Introduction

Increasing heat flux of electronic components in fields requiring high technology such as aeronautics, medicine, defense, and aerospace makes two-phase cooling practices where less surface temperature rise is seen more and more convenient. The fact that electronic components have become more compact, and smaller in dimensions, has led to a significant increase in the amount of heat emitted per unit area of such components [1-5]. It is inevitably important to rapidly and effectively remove the high heat fluxes produced by such components to ensure efficient lifecycle and performance. Hence, thanks to higher ratios of heat transfer surface area to volume, and lower requirement for fluids, micro-channels are now an important alternative [6-9]. Micro-channels have higher ratios of heat transfer area to volume, allowing a higher amount of heat transfer on smaller surfaces, which, in turn require a lower amount of fluid [10-14]. To increase the heat transfer performance of micro-channels, the use of thermally enhanced fluids is now more preferrable. Such fluids, obtained by blending fluid with nanoparticles with higher thermal conductivity than that of standard fluids, are called nanofluids. Nanofluids, formed using special methods, are not simple solid-liquid suspensions with improved thermal properties, but act like a single-phase fluid with high stability and no sedimentation tendency [15-19]. In most studies, researchers have placed great importance on increasing the

* Author's e-mail: hsimsek@nku.edu.tr

heat transfer performance, with continuing efforts to obtain and use the fluids for more efficiency [20-24]. Compared to other fluids, nanofluids have been emerging recently, and becoming increasingly popular in recent years for heat transfer practices. Nanofluids are obtained through the homogeneous dispersion of nanosized metals, metal oxides, carbon nanotube particles into conventional heat transfer fluids. The most important advantage of such fluids is the achievement of stabilization as it is the only way that thermal performance tends to increase [25-27]. Nanoparticles added to pure fluids, used in heat transfer practices, contributes to the thermophysical properties of the fluid, and consequently, results in significant improvement in heat transfer. One of the main reasons of such improvement in heat transfer using nanofluids is the increase in the heat transfer coefficient of the fluid [28-32]. This increase in heat transfer with the use of nanofluids leads most of the research on nanofluids to study the thermal conductivity coefficient of nanofluids and the positive development of heat transfer with nanofluids [33, 34]. Micro-channels with their significant potential to remove excess heat resulting from the surface area to volume ratio on small areas, would allow the design of high efficiency heat exchangers, thanks to their use in combination with nanofluids with improved thermal properties, rather than conventional thermal heat transfer fluids with insufficient thermophysical properties and thermal conductivity [35-37]. In a study, nanofluids (0.2-1.0%) were produced from Boehmite nanoparticles, composed of 50% water and 50% ethylene glycol, and with different particle shapes and used as the working fluid in a double-pipe heat exchanger. Buffers were placed at different angles on the flow area and the highest heat transfer coefficient obtained under laminar flow conditions was at 20° buffer angle and with cylindrical particles [38]. Another study using nanofluids in heat exchangers analyses CuO-water and TiO_2-water nanofluids in a helical coil heat exchanger under laminar flow conditions, using CFD method. In the study, where the highest volumetric concentration is 2.0%, the highest heat exchanger efficiency achieved at this concentration is found to be 90% with CuO-water nanofluid. Nusselt number is observed to have increased by 97% under the same conditions [39].

This research aims to study the slip flow of nanofluids in a microtube, heated with a constant heat flux, analytically. The results from the study are analyzed to find out the effectiveness of water-based nanofluids, Cu, CuO, and Al_2O_3 on fluid-flow and heat transfer.

Analysis

The geometry and co-ordinate system of the microtube are given in fig. 1. It is assumed that the nanofluid in the pipe is laminar flow and incompressible. It is also assumed that the nanofluid is a fully developed flow with stable thermo-physical properties. A single-phase approach was used to model both fluid-flow and heat transfer. The purpose of using a single-phase approach here is because nanoparticles are very small in size and can be fluidized very easily. The thermal equilibrium condition is accepted for fluid particles and nanoparticles. Therefore, it is assumed that fluid particles and nanoparticles flow at the same velocity. The z-axis represents and is through centerline of the micropipe and the r-axis is perpendicular to it. The equations with viscous diffusions used in the study are:

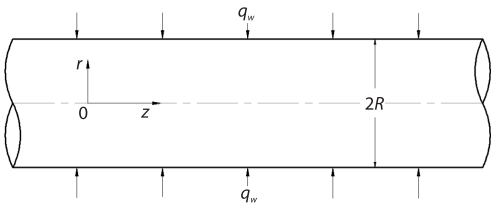

Figure 1. Geometry and the co-ordinate system

Examples of centered formulas:

$$\frac{\mathrm{d}^2 u}{\mathrm{d}r^2} = \frac{1}{\mu_{\mathrm{nf}}} \frac{\mathrm{d}p}{\mathrm{d}z} \tag{1}$$

$$u\frac{\partial T}{\partial z}=\alpha_{\mathrm{nf}}\frac{\partial^2 T}{\partial r^2}+\frac{\mu_{nf}}{\left(\rho c_p\right)_{\mathrm{nf}}}\left(\frac{\partial u}{\partial r}\right)^2 \tag{2}$$

where u, ρ, T, μ, c_p, and α are the dimensional component of velocity in the z-axis, dimensional pressure, the temperature, the viscosity of the fluid, the heat capacity, and the thermal dissipation, respectively. The viscosity of nanofluids is usually estimated using the following formula suggested by [40] for a two-phase mixture. In this study, the model [40] is used:

$$\mu_{\mathrm{nf}}=\frac{\mu_{\mathrm{f}}}{\left(1-\phi\right)^{2.5}} \tag{3}$$

The nanofluid thermal diffusion coefficient is defined:

$$\alpha_{\mathrm{nf}}=\frac{k_{\mathrm{nf}}}{\left(\rho c_p\right)_{\mathrm{nf}}} \tag{4}$$

In order to determine the heat transfer coefficients of nanofluids, the models proposed in the literature for solid-liquid mixtures with micron-sized particles are used. In this study, the model by [41], which states that the base liquid should contain solid particles and solid-like nanolayers, and that the solid-like nanoparticle acts as a thermal bridge between the solid nanoparticle and the base fluid, and includes the liquid layering effect on the nanoparticles:

$$\frac{k_{\mathrm{nf}}}{k_{\mathrm{f}}}=\frac{k_{\mathrm{s}}+2k_{\mathrm{f}}+2\left(k_{\mathrm{s}}-k_{\mathrm{f}}\right)\left(1+\beta\right)^3\phi}{k_{\mathrm{s}}+2k_{\mathrm{f}}-\left(k_{\mathrm{s}}-k_{\mathrm{f}}\right)\left(1+\beta\right)^3\phi} \tag{5}$$

where β is defined as the ratio of the liquid layer thickness to the nanoparticle radius [42]. Defines the thermal capacity of nanofluids:

$$\left(\rho c_p\right)_{\mathrm{nf}}=\left(1-\phi\right)\left(\rho c_p\right)_{\mathrm{nf}}+\phi\left(\rho c_p\right)_{\mathrm{p}} \tag{6}$$

The boundary conditions for slip rate and temperature jump for a stationary wall are given in eqs. (8) and (9), respectively:

$$u_{\mathrm{s}}-u_{\mathrm{w}}=-\left(\frac{2-\sigma}{\sigma}\right)\lambda\left.\frac{\partial u}{\partial r}\right|_{r=r_0} \tag{7}$$

where u_{s} and u_{w} are the slip rate of the fluid on the wall and the velocity of the wall, respectively:

$$T_{\mathrm{s}}-T_{\mathrm{w}}=-\left(\frac{2-\sigma_t}{\sigma_t}\right)\left(\frac{2\gamma}{\mathrm{Pr}\left(\gamma+1\right)}\right)\lambda\left.\frac{\partial T}{\partial r}\right|_{r=r_0} \tag{8}$$

where T_{s} and T_{w} are the temperature of the fluid on the wall and the temperature of the wall, while σ and σ_t are the tangential momentum coefficient and the thermal cohesion coefficient, respectively.

Velocity profile

Dimensionless variables used in the study:

$$U=\frac{u}{u_{\mathrm{m,f}}},\ U_{\mathrm{s}}=\frac{u_s}{u_{\mathrm{m,f}}},\ R=\frac{r}{r_0},\ Z=\frac{z}{r_0},\ P=\frac{pR_0}{\mu_{\mathrm{f}}u_{\mathrm{m,f}}},\ \mathrm{Kn}=\frac{\lambda}{2r_0} \tag{9}$$

where $\mu_{\mathrm{m,f}}$ is the average velocity of the base fluid.

The dimensionless momentum equation in the *x*-direction and the necessary boundary conditions are obtained:

$$\frac{\mathrm{d}^2U}{\partial R^2} = \frac{\mu_\mathrm{f}}{\mu_\mathrm{nf}}\frac{\mathrm{d}P}{\mathrm{d}Z} \tag{10}$$

$$uY = 0, \quad \left.\frac{\mathrm{d}U}{\mathrm{d}R}\right|_{R=0} = 0 \tag{11}$$

$$Y = 1, \; U = U_\mathrm{s} = -2\mathrm{Kn}\left.\frac{\mathrm{d}U}{\mathrm{d}R}\right|_{R=1} \tag{12}$$

Given the boundary conditions in eqs. (10)-(12) the analytical solution the equation:

$$U = \frac{\mu_\mathrm{f}}{\mu_\mathrm{nf}}\frac{8\mathrm{Kn} + 2\left(1 - R^2\right)}{1 + 8\mathrm{Kn}} \tag{13}$$

Temperature distribution

The dimensionless temperature:

$$\theta = \frac{T - T_\mathrm{s}}{\dfrac{q_\mathrm{w} r_0}{k_\mathrm{f}}} \tag{14}$$

Dimensionless energy equation:

$$\frac{\mathrm{d}}{\mathrm{d}R}\left(R\frac{\mathrm{d}\theta}{\mathrm{d}R}\right) = \frac{k_\mathrm{f}}{k_\mathrm{nf}}\frac{\mu_\mathrm{f}}{\mu_\mathrm{nf}} \cdot$$
$$\cdot\left[\frac{\left(\rho c_p\right)_\mathrm{nf}}{\left(\rho c_p\right)_\mathrm{f}} a \frac{2\left(R - R^3 + 4\mathrm{Kn}R\right)}{\left(1 + 8\mathrm{Kn}\right)} - \frac{2\left(R - R^3 + 4\mathrm{Kn}R\right)}{\left(1 + 8\mathrm{Kn}\right)} - 32\mathrm{Br}\frac{R^3}{\left(1 + 8\mathrm{Kn}\right)^2}\right] \tag{15}$$

where *a* is represented:

$$a = \frac{u_\mathrm{m,f} r_0 \left(\rho c_p\right)_\mathrm{f}}{q_\mathrm{w}} \tag{16}$$

where Br, on the other hand, represents the modified Bbrinkman number:

$$\mathrm{Br} = \frac{\mu_\mathrm{f} u_\mathrm{m,f}^2}{q_\mathrm{w} D} \tag{17}$$

The energy equation is applied to the following boundary conditions:

$$R = 0, \quad \left.\frac{\partial\theta}{\partial R}\right|_{R=0} = 0 \tag{18}$$

$$R = 1, \quad \left.\frac{\partial\theta}{\partial R}\right|_{R=1} = \frac{k_\mathrm{f}}{k_\mathrm{nf}} \tag{19}$$

The solution of eq. (15) under thermal boundary conditions:

$$\theta(R)=\frac{T-T_{\mathrm{s}}}{\frac{q_{\mathrm{w}}r_0}{k_{\mathrm{f}}}}=\frac{k_{\mathrm{f}}}{k_{\mathrm{nf}}}\left[\frac{4}{(1+8\mathrm{Kn})}+\frac{\mu_{\mathrm{f}}}{\mu_{\mathrm{nf}}}\frac{32\mathrm{Br}}{(1+8\mathrm{Kn})^3}\right]\cdot$$
$$\cdot\left[\frac{R^2}{4}-\frac{R^4}{16}+\mathrm{Kn}\left(R^2-1\right)-\frac{3}{16}\right]-\frac{k_{\mathrm{f}}}{k_{\mathrm{nf}}}\frac{\mu_{\mathrm{f}}}{\mu_{\mathrm{nf}}}\frac{2Br}{(1+8\mathrm{Kn})^2}\left(R^4-1\right) \tag{20}$$

Equation 20 is denominated by T_{s} and converted to an equation nominated by T_{w}, using conversion formula:

$$\frac{T-T_{\mathrm{w}}}{\frac{q_{\mathrm{w}}r_0}{k_{\mathrm{f}}}}=-2\frac{k_{\mathrm{f}}}{k_{\mathrm{nf}}}\frac{\mathrm{Kn}}{\mathrm{Pr}} \tag{21}$$

after which the eq. (22) becomes:

$$\tilde{\theta}=\frac{T-T_{\mathrm{w}}}{\frac{q_{\mathrm{w}}r_0}{k_{\mathrm{f}}}}=\frac{k_{\mathrm{f}}}{k_{\mathrm{nf}}}\left\{\left[\frac{4}{(1+8\mathrm{Kn})}+\frac{\mu_{\mathrm{f}}}{\mu_{\mathrm{nf}}}\frac{32\mathrm{Br}}{(1+8\mathrm{Kn})^3}\right]\left[\frac{R^2}{4}-\frac{R^4}{16}+\mathrm{Kn}\left(R^2-1\right)-\frac{3}{16}\right]-\right.$$
$$\left.-\frac{\mu_{\mathrm{f}}}{\mu_{\mathrm{nf}}}\frac{2\mathrm{Br}}{(1+8\mathrm{Kn})^2}\left(R^4-1\right)-\frac{4\gamma}{\gamma+1}\frac{\mathrm{Kn}}{\mathrm{Pr}}\right\} \tag{22}$$

In fully developed flows, the Nusselt number is defined by the mean fluid temperature. The average temperature is represented:

$$T_{\mathrm{m,nf}}=\frac{\int\rho uT\mathrm{d}A}{\int\rho T\mathrm{d}A} \tag{23}$$

The dimensionless average temperature in modified Brinkman is obtained:

$$\tilde{\theta}_{\mathrm{m,nf}}=\frac{T_{\mathrm{m,nf}}-T_{\mathrm{w}}}{\frac{q_{\mathrm{w}}r_0}{k_{\mathrm{f}}}}=\frac{8}{(1+8\mathrm{Kn})^2}\frac{k_{\mathrm{f}}}{k_{\mathrm{nf}}}\left[-2\mathrm{Kn}^2-\frac{8\mathrm{Kn}}{12}-\frac{11}{192}\right]+\frac{64\mathrm{Br}}{(1+8\mathrm{Kn})^4}\frac{k_{\mathrm{f}}}{k_{\mathrm{nf}}}\frac{\mu_{\mathrm{f}}}{\mu_{\mathrm{nf}}}\cdot$$
$$\cdot\left[-2\mathrm{Kn}^2-\frac{8\mathrm{Kn}}{12}-\frac{11}{192}\right]-\frac{4\mathrm{Br}}{(1+8\mathrm{Kn})^3}\frac{k_{\mathrm{f}}}{k_{\mathrm{nf}}}\frac{\mu_{\mathrm{f}}}{\mu_{\mathrm{nf}}}\left[-\frac{8\mathrm{Kn}}{3}-\frac{5}{12}\right]-\frac{4\gamma}{\gamma+1}\frac{k_{\mathrm{f}}}{k_{\mathrm{nf}}}\frac{\mathrm{Kn}}{\mathrm{Pr}} \tag{24}$$

The forced convection heat transfer coefficient is represented:

$$h_{\mathrm{nf}}=\frac{q_{\mathrm{w}}}{T_{\mathrm{w}}-T_{\mathrm{m,nf}}} \tag{25}$$

after which the average Nusselt number is represented:

$$\mathrm{Nu}=-\frac{2}{\tilde{\theta}_{\mathrm{m,nf}}} \tag{26}$$

Finally, when the dimensionless average temperature substituted, the average Nusselt number is represented:

$$\mathrm{Nu} = -2\left\{\frac{8}{\left(1+8\mathrm{Kn}\right)^2}\frac{k_\mathrm{f}}{k_\mathrm{nf}}\left[-2\mathrm{Kn}^2-\frac{8\mathrm{Kn}}{12}-\frac{11}{192}\right]+\frac{64\mathrm{Br}}{\left(1+8\mathrm{Kn}\right)^4}\frac{k_\mathrm{f}}{k_\mathrm{nf}}\frac{\mu_\mathrm{f}}{\mu_\mathrm{nf}}\cdot\right.$$
$$\left.\cdot\left[-2\mathrm{Kn}^2-\frac{8\mathrm{Kn}}{12}-\frac{11}{192}\right]-\frac{4\mathrm{Br}}{\left(1+8\mathrm{Kn}\right)^3}\frac{k_\mathrm{f}}{k_\mathrm{nf}}\frac{\mu_\mathrm{f}}{\mu_\mathrm{nf}}\left[-\frac{8\mathrm{Kn}}{3}-\frac{5}{12}\right]-\frac{4\gamma}{\gamma+1}\frac{k_\mathrm{f}}{k_\mathrm{nf}}\frac{\mathrm{Kn}}{\mathrm{Pr}}\right\}^{-1} \quad (27)$$

Analysis

Thermo-physical properties of pure water, Cu, CuO, and Al_2O_3 are shown in tab. 1. Three different nanoparticles solid volume values, 0, 0.04, and 0.08, were used. For values between 0 and 0.04 of the Knudsen number, the Brinkman number, solid volume ratio, and the ratio of liquid layer thickness to nanoparticle radius were calculated. The Brinkman number was between –0.1 and 0.1, the solid volume ratio was between 0 and 0.08, and the ratio of liquid layer thickness to nanoparticle radius was between 0 and 0.4. Water was taken as the working fluid with Pr = 6.2 and Cu, CuO, and Al_2O_3 as the nanoparticles.

Table 1. Thermo-physical properties of Cu, CuO, Al_2O_3 and water

Property	Water	Cu	CuO	Al_2O_3
ρ [kgm^{-3}]	997.1	8933	6500	3970
c_p [Jkg^{-1}K^{-1}]	4179	385	535.6	765
k [Wm^{-1}K^{-1}]	0.613	400	20	40

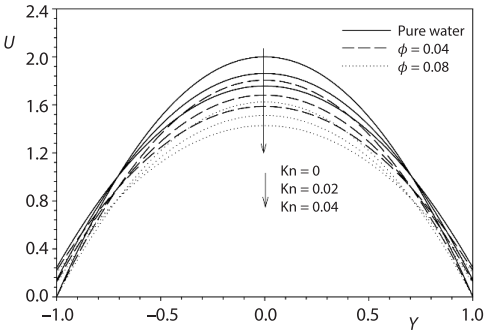

Figure 2. Velocity profile

The axial dimensionless velocity profile for various values of the slip factor and solid volume ratio (ϕ = 0.04 and ϕ = 0.08) is shown in fig. 2.

As the slip factor, Kn, increases, the slip velocity on the walls increases, while the velocity in the core region gradually decreases. However, with the increase of the solid volume in nanoparticles, the velocity decreases, while the sliding velocity on the wall increases. The increase in the nanoparticle volume leads to an increase in the viscous forces of the nanofluid. Due to the increase in viscous forces acting opposite the nanofluid, the fluid velocity decreases. Therefore, viscous forces increase, and it is observed that as the nanoparticle volume increases, the velocity decreases. When the solid volume rate is ϕ = 0, the base fluid is formed, and the velocity increases, which is clearly shown in tab. 2.

As the Knudsen number increases, the temperature jump on the micro-channel walls increases, and as a result, the Nusselt number decreases, which in turn, reduces the heat transfer. For viscous dissipation Br < 0, the fluid is cooled by the cold wall, while for Br = 0, where viscous dissipation is neglected, and Br > 0, the fluid is heated by the hot wall. Reviewing figs. 3-5, the graphs for Cu, CuO, and Al_2O_3, for the negative values of the Brinkman number, indicate that the temperature jump increases and the average Nusselt number decreases as the

Table 2. Slip rates occurring in the core and on the walls for various values of slip factor and solid volume rate

Kn	U					
	Pure water		$\phi = 0.04$		$\phi = 0.08$	
	$Y = 0$	$Y = \pm 1$	$Y = 0$	$Y = \pm 1$	$Y = 0$	$Y = \pm 1$
0	2.0000	0	1.8060	0	1.6237	0
0.02	1.8621	0.1379	1.6814	0.1245	1.5117	0.1120
0.04	1.7576	0.2424	1.5877	0.2189	1.4269	0.1968

Knudsen number increases. Consequently, the decrease in the Nusselt number has negative effect on the heat transfer. However, the introduction of nanosized particles to the flow area ($\phi = 0.04$, $\phi = 0.08$) increases the heat transfer. When the nanoparticle rate is increased from 4% to 8%, the Nusselt number becomes higher as indicated tabs. 3-9. The increase in the Nusselt number also provides a significant increase in heat transfer by increasing the ratio of the liquid layer thickness to the nanoparticle radius. The increase in heat transfer is clearly seen both figs. 3-5 and tabs. 3-9. This is also applicable for the positive values of Brinkman number.

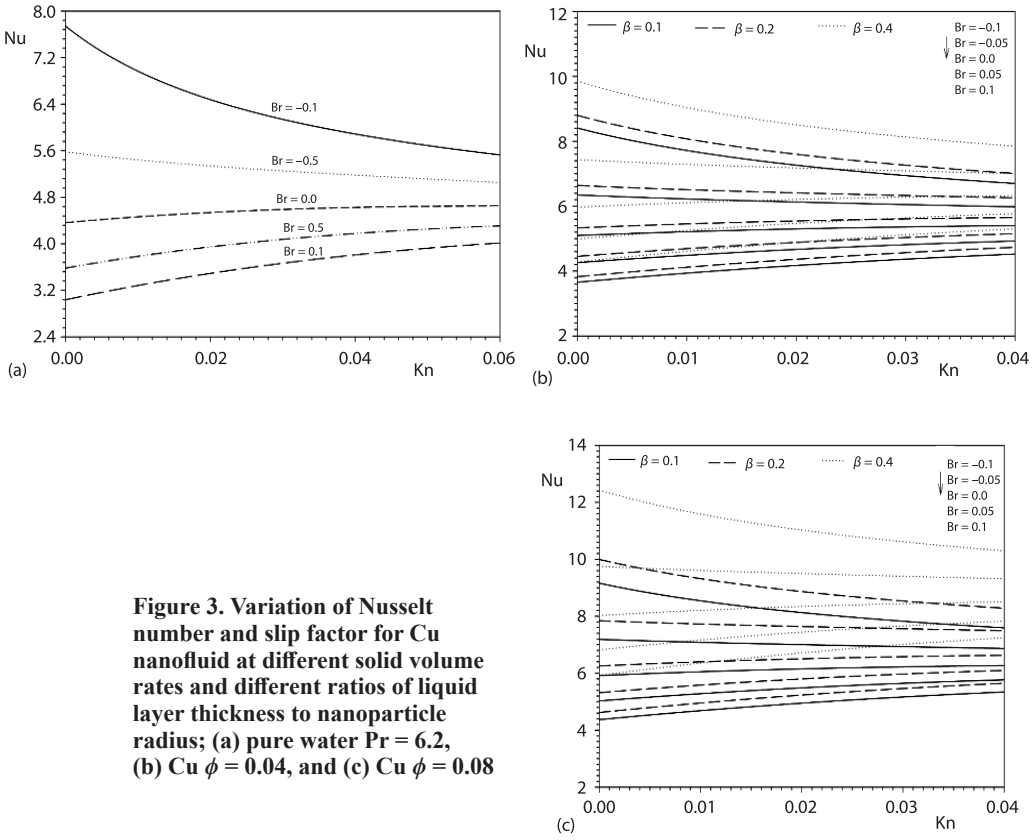

Figure 3. Variation of Nusselt number and slip factor for Cu nanofluid at different solid volume rates and different ratios of liquid layer thickness to nanoparticle radius; (a) pure water Pr = 6.2, (b) Cu $\phi = 0.04$, and (c) Cu $\phi = 0.08$

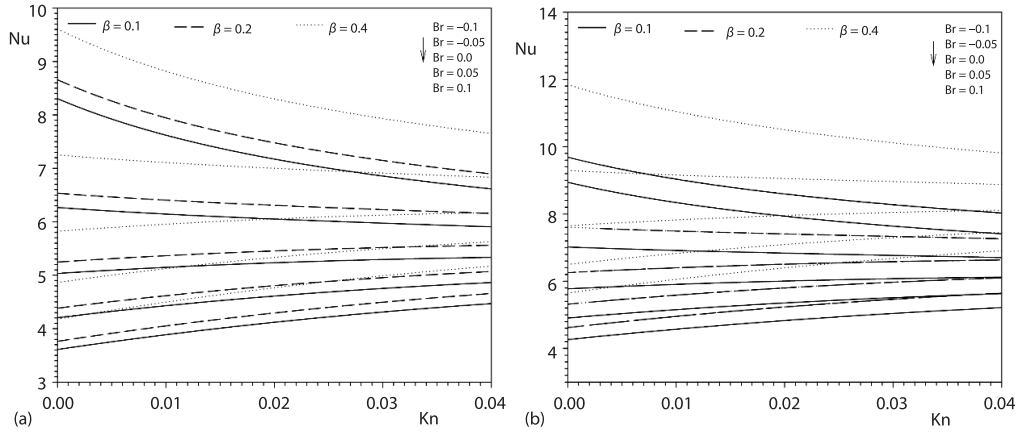

Figure 4. Variation of Nusselt number and slip factor for CuO nanofluid at different solid volume rates and different ratios of liquid layer thickness to nanoparticle radius; (a) CuO $\phi = 0.04$ and (b) CuO $\phi = 0.08$

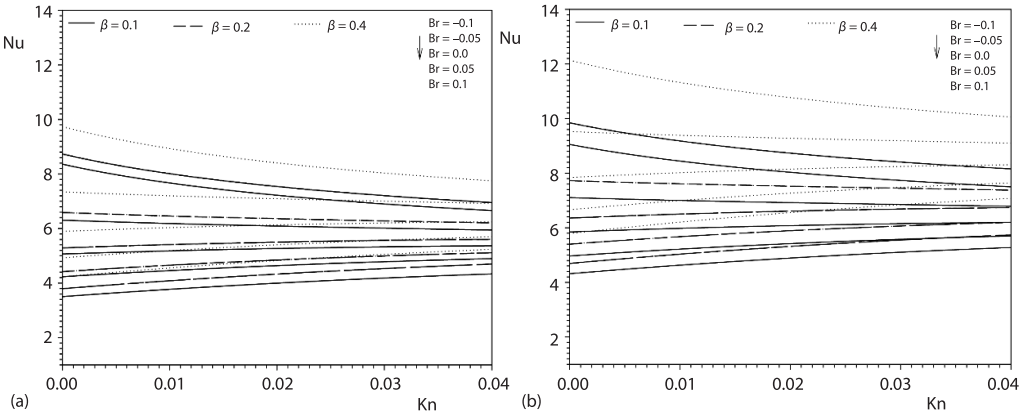

Figure 5. Variation of Nusselt number and slip factor for Al_2O_3 nanofluid at different solid volume rates and different ratios of liquid layer thickness to nanoparticle radius; (a) Al_2O_3 $\phi = 0.04$ and (b) Al_2O_3 $\phi = 0.08$

Table 3. Fully developed Nusselt number for different values of Knudsen and Brinkman numbers for pure water

Kn	Br = –0.1	Br = 0	Br = 0.1
0.0	7.7419	4.3636	3.0380
0.02	6.4777	4.5375	3.4910
0.04	5.8873	4.6250	3.8084

Table 4. Fully developed Nusselt number $\phi = 0.04$ for different values of Knudsen and Brinkman numbers for Cu

Kn	Br = –0.1			Br = 0			Br = 0.1		
	$\beta = 0.1$	$\beta = 0.2$	$\beta = 0.4$	$\beta = 0.1$	$\beta = 0.2$	$\beta = 0.4$	$\beta = 0.1$	$\beta = 0.2$	$\beta = 0.4$
0.0	8.4100	8.7972	9.8509	5.0912	5.3309	5.9693	3.6558	3.8241	4.2821
0.02	7.2638	7.5983	8.5083	5.2993	5.5433	6.2072	4.1771	4.3632	4.8858
0.04	6.6983	7.0067	7.8459	5.4014	5.6502	6.3269	4.5253	4.7337	5.3006

Table 5. Fully developed Nusselt number $\phi = 0.08$ for different values of Knudsen and Brinkman numbers for Cu

Kn	Br = –0.1			Br = 0			Br = 0.1		
	$\beta = 0.1$	$\beta = 0.2$	$\beta = 0.4$	$\beta = 0.1$	$\beta = 0.2$	$\beta = 0.4$	$\beta = 0.1$	$\beta = 0.2$	$\beta = 0.4$
0.0	9.1610	9.9923	12.4260	5.9157	6.2554	8.0240	4.3682	4.6191	5.9250
0.02	8.1277	8.8652	11.0244	6.1514	6.5040	8.3437	4.9482	5.2323	6.7117
0.04	7.5914	8.2803	10.2970	6.2700	6.6300	8.5046	5.3404	5.6471	7.2437

Table 6. Fully developed Nusselt number $\phi = 0.04$ for different values of Knudsen and Brinkman numbers for CuO

Kn	Br = –0.1			Br = 0			Br = 0.1		
	$\beta = 0.1$	$\beta = 0.2$	$\beta = 0.4$	$\beta = 0.1$	$\beta = 0.2$	$\beta = 0.4$	$\beta = 0.1$	$\beta = 0.2$	$\beta = 0.4$
0.0	8.3052	8.6568	9.6081	5.0327	5.2458	5.82226	3.6102	3.7630	4.1766
0.02	7.1734	7.4770	8.2986	5.2333	5.4548	6.0542	4.1192	4.2935	4.7654
0.04	6.6149	6.8949	7.6526	5.3342	5.5600	6.1709	4.4689	4.6581	5.1700

Table 7. Fully developed Nusselt number $\phi = 0.08$ for different values of Knudsen and Brinkman numbers for CuO

Kn	Br = –0.1			Br = 0			Br = 0.1		
	$\beta = 0.1$	$\beta = 0.2$	$\beta = 0.4$	$\beta = 0.1$	$\beta = 0.2$	$\beta = 0.4$	$\beta = 0.1$	$\beta = 0.2$	$\beta = 0.4$
0.0	8.9416	9.6871	11.8416	5.7739	6.2554	6.4960	4.2636	4.6191	5.6664
0.02	7.9333	8.5945	10.5059	6.0040	6.5046	7.9513	4.8296	5.2323	6.3960
0.04	7.4095	8.0274	9.8127	6.1198	6.6300	8.1046	5.2124	5.6471	6.9030

Table 8. Fully developed Nusselt number $\phi = 0.04$ for different values of Knudsen and Brinkman numbers for Al_2O_3

Kn	Br = –0.1			Br = 0			Br = 0.1		
	$\beta = 0.1$	$\beta = 0.2$	$\beta = 0.4$	$\beta = 0.1$	$\beta = 0.2$	$\beta = 0.4$	$\beta = 0.1$	$\beta = 0.2$	$\beta = 0.4$
0.0	8.3588	8.7285	9.7318	5.0652	5.2692	5.8972	3.5034	3.7942	4.2303
0.02	7.2196	7.5390	7.0911	5.2670	5.5000	6.1322	3.9973	4.3291	4.8267
0.04	6.6575	6.9520	7.7511	5.3686	5.6060	5.6987	4.3367	4.6967	5.2366

Table 9. Fully developed Nusselt number $\phi = 0.08$ for different values of Knudsen and Brinkman numbers for Al_2O_3

Kn	Br = –0.1			Br = 0			Br = 0.1		
	$\beta = 0.1$	$\beta = 0.2$	$\beta = 0.4$	$\beta = 0.1$	$\beta = 0.2$	$\beta = 0.4$	$\beta = 0.1$	$\beta = 0.2$	$\beta = 0.4$
0.0	9.0534	9.8424	9.5249	5.8462	6.3557	7.8378	4.3169	4.6931	5.7875
0.02	8.0322	8.7323	10.7685	6.0791	6.6089	8.1501	4.8900	5.3162	6.5559
0.04	7.5022	8.1561	10.0580	6.1963	6.7363	8.3072	5.2777	5.7376	7.0756

For the positive values of the Brinkman number, the temperature difference between the wall and the fluid is small. Therefore, the Nusselt number becomes lower as a result of an increase in the Brinkman number. For the negative values of the Brinkman number, on the other

hand, the Nusselt number becomes higher as a result of the negative increase of the Brinkman number, as the temperature difference between the wall and the fluid is large. The Nusselt number becomes much higher for higher ratios of liquid layer thickness to nanoparticle radius. For nanoparticles with higher thermal conductivity, the Nusselt number is higher. For nanoparticles, Cu has the highest value while CuO has the lowest value.

The variation of the average Nusselt number with the slip factor against various values of the Brinkman number for Cu, CuO, and $A_{l2}O_3$, the solid volume rate, and the ratio of liquid layer thickness to nanoparticle radius is shown figs. 6-8.

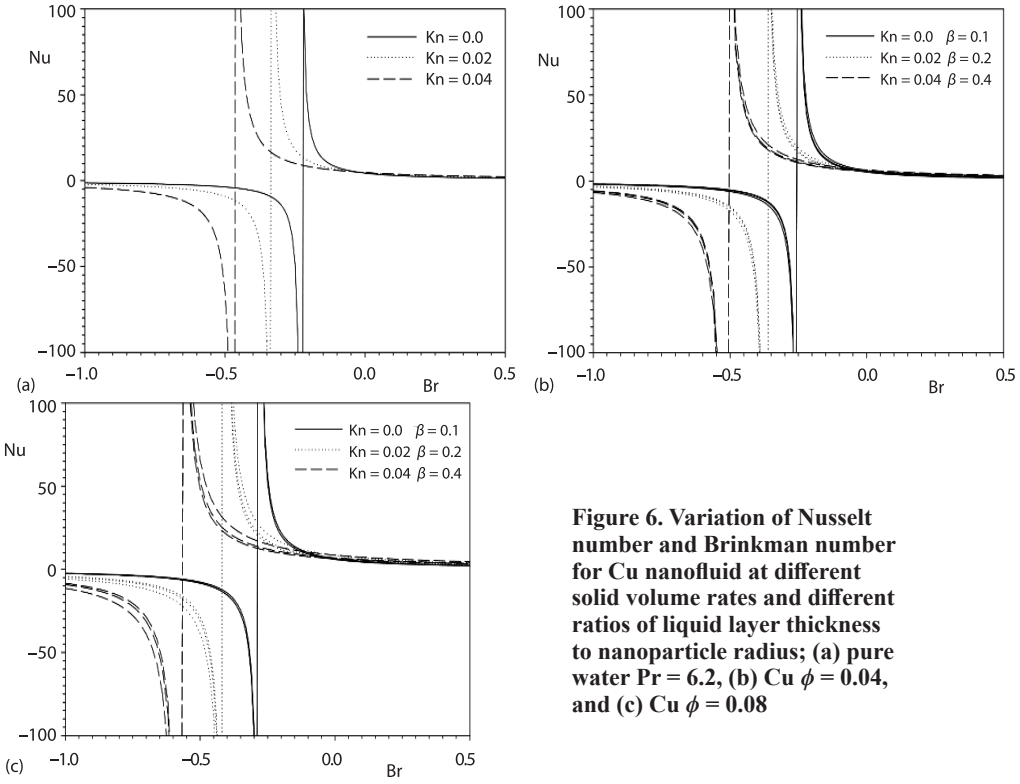

Figure 6. Variation of Nusselt number and Brinkman number for Cu nanofluid at different solid volume rates and different ratios of liquid layer thickness to nanoparticle radius; (a) pure water Pr = 6.2, (b) Cu ϕ = 0.04, and (c) Cu ϕ = 0.08

Reviewing figs. 6-8, it can be seen that some values of the Brinkman number, there are direction changes and discontinuity points in Nusselt number. As the Knudsen number increases, the Nusselt number decreases, however, as the ratio of the liquid layer thickness to the nanoparticle radius increases, the Nusselt number, as result of the positive increase in the Brinkman number, increases. As the Knudsen number increases, the Nusselt number decreases, and as the ratio of the liquid layer thickness to the nanoparticle radius increases, the Nusselt number, as result of the negative increase in the Brinkman number, decreases. After a certain value, the Nusselt number reaches 0 and a discontinuity occurs. After such point where the discontinuity occurs, it is seen that the Nusselt number decreases or increases again. The change in direction occurring in the Nusselt number indicates that the heat released as a result of viscous diffusion equals the heat flux that tends to transfer from the channel wall to the fluid. There is no heat transfer at this point. After this point, the direction of heat transfer changes. With the further increase of viscous dissipation, the bulk temperature comes into equilibrium with the channel wall temperature and a discontinuity occurs [42].

Reviewing figs. 6-8, the increase in the solid volume rate ϕ (from $\phi = 0.04$ to $\phi = 0.08$) has changed the discontinuity points. Increasing the value of ϕ leads to discontinuity points at lower Brinkman numbers. These discontinuity points are formed at lower viscous dissipation values, in other words, at lower Brinkman numbers, as the Knudsen number value increased. The change in the Nusselt number yields similar results for the nanofluids, Cu, CuO, and Al_2O_3. In the case of using different nanofluids, only the values will change in the Nusselt number, but the behavior will remain the same.

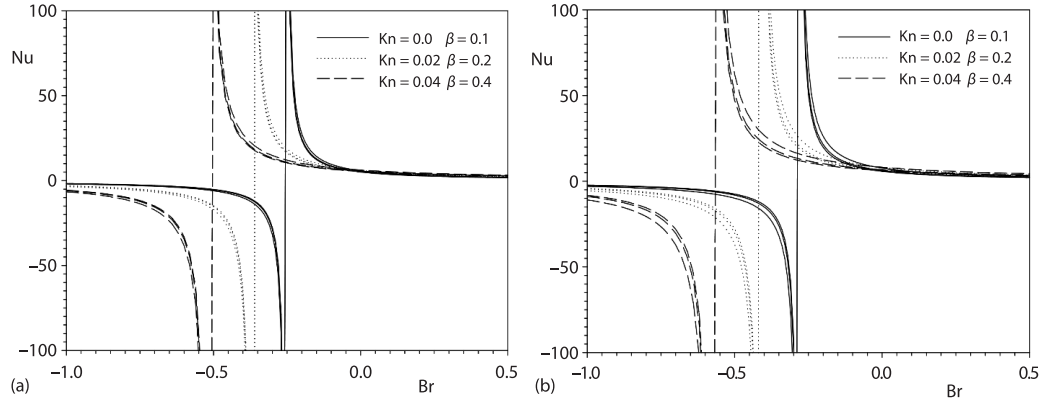

Figure 7. Variation of Nusselt number and Brinkman number for CuO nanofluid at different solid volume rates and different ratios of liquid layer thickness to nanoparticle radius; (a) CuO $\phi = 0.04$ and (b) CuO $\phi = 0.08$

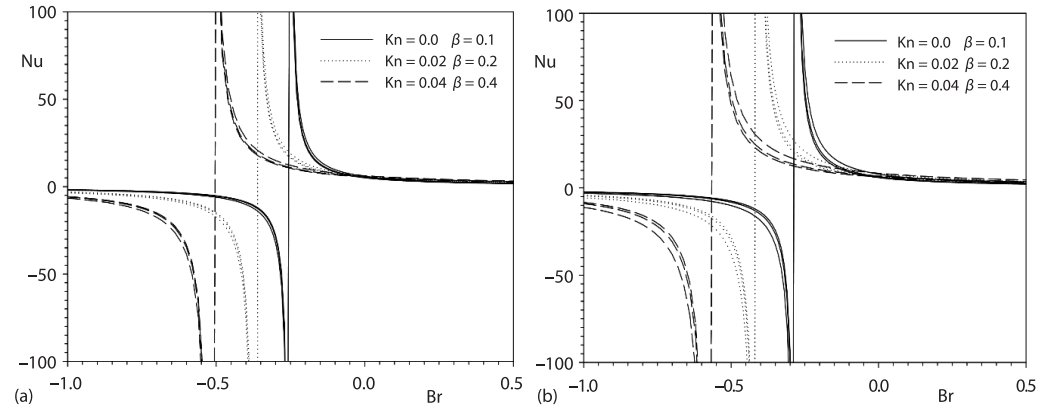

Figure 8. Variation of Nusselt number and Brinkman number for Al_2O_3 nanofluid at different solid volume rates and different ratios of liquid layer thickness to nanoparticle radius; (a) Al_2O_3 $\phi = 0.04$ and (b) Al_2O_3 $\phi = 0.08$

Conclusions

In this research, the slip flow of water, as base fluid, and the nanofluids, Cu, CuO, and Al_2O_3 as nanoparticles are analytically studies in a micro pipe, heated with constant heat flux. The effects of Brinkman number and Knudsen number on Nusselt number are analyzed at different values of the solid volume rate and the ratio of liquid layer thickness to nanoparticle radius. The significant results obtained in this study are as follows.

- The addition of nanoparticles to the flow field caused a significant change in slip rate. When nanoparticles are added to the base fluid water, the velocity in the core and the slip rate on the walls tend to decrease. Decrease in the share rate on the walls is observed to be higher when the nanoparticle volume rate is increased from 4-8%, which indicates that the use of nanoparticles has a significant effect on the velocity.
- The addition of nanoparticles to the flow area led to a significant increase in heat transfer. Heat transfer increases as the particle volumetric concentration increases, and for higher ratios of liquid layer thickness to nanoparticle radius, heat transfer also becomes higher.
- For the nanoparticles, Cu, CuO, and Al_2O_3, the highest heat transfer improvement is with Cu, Al_2O_3, and CuO, respectively.

In conclusion, the Nusselt number is higher for nanoparticles with higher thermal conductivity. Therefore, nanoparticles with higher thermal conductivity have an important role in improving heat transfer.

Nomenclature

Br – modified Brinkman number
c_p – specific heat at constant pressure, [$kg^{-1}K^{-1}$]
h – convective heat transfer coefficient, [$Wm^{-2}K^{-1}$]
Kn – Knudsen number
k – thermal conductivity, [$Wm^{-1}K^{-1}$]
Nu – Nusselt number
P – pressure, [Pa]
Pr – Prandtl number
q_w – wall heat flux, [Wm^{-2}]
R – dimensionless radial co-ordinate, [m]
r – radial direction, [m]
T – temperature, [K]
U – velocity, [ms^{-1}]
Z – dimensionless axial direction
z – axial direction, [m]

Greek symbols

α – thermal diffusivity, [m^2s^{-1}]
β – ratio of the liquid layering thickness to the nanoparticle radius
θ – dimensionless temperature
$\tilde{\theta}$ – dimensionless temperature
μ – dynamic viscosity, [Pa·s]
ρ – density, [kgm^{-3}]
ϕ – solid volume fraction

Subscripts

f – base fluid layer solid-like nanolayer
m – mean
nf – nanofluid
s – solid nanoparticles or slip
w – wall

References

[1] Li, Y.-X., *et al*., Simultaneous Features of Wu's Slip, Non-Linear Thermal Radiation and Activation Energy in Unsteady Bioconvective Flow of Maxwell Nanofluid Configured by a Stretching Cylinder, *Chinese Journal of Physics*, *73* (2021), Oct., pp. 462-478
[2] Monavari, A., *et al*., Thermohydraulic Performance of a Nanofluid in a Micro-Channel Heat Sink: Use of Different Micro-Channels for Change in Process Intensity, *Journal of the Taiwan Institute of Chemical Engineers*, *125* (2021), Aug., pp. 1-14
[3] Ritchey, S. N., *et al*., Local Measurement of Flow Boiling Heat Transfer in an Array of Non-Uniformly Heated Micro-Channels, *International Journal of Heat and Mass Transfer*, *71* (2014), Apr., pp. 206-216
[4] Kandlikar, S. G., *et al*., Heat Transfer in Micro-Channels-2012 Status and Research Needs, *Journal of Heat Transfer*, *135* (2013), 9, 091001
[5] Kandlikar, S. G., Mechanistic Considerations for Enhancing Flow Boiling Heat Transfer in Micro-Channels, *Journal of Heat Transfer*, *1338* (2016), 2, 021504
[6] Ozer, *et al*., Effects od Fusel Oil Use in a Thermal Coated Engine, *Fuel*, *306* (2021), 121716
[7] Rabiei, S., *et al*., Thermal and Hydraulic Characteristics of a Hybrid Nanofluid Containing Graphene Sheets Decorated with Platinum through a New Wavy Cylindrical Micro-Channel, *Applied Thermal Engineering*, *181* (2020), 115981
[8] Ghadirzadeh, S., Kalteh, M., Lattice Boltzmann Simulation of Temperature Jump Effect on the Nanofluid Heat Transfer in an Annulus Micro-Channel, *International Journal of Mechanical Sciences*, *133* (2017), Nov, pp. 524-534

[9] Mathew, A., *et al*., Significance of Multiple Slip and Nanoparticle Shape on Stagnation Point Flow of Silver-Blood Nanofluid in the Presence of Induced Magnetic Field, *Surfaces and Interfaces*, *25* (2021), Aug., 101267
[10] Bahiraei, M., *et al*., Irreversibility Characteristics of a Modified Micro-Channel Heat Sink Operated with Nanofluid Considering Different Shapes of Nanoparticles, *International Journal of Heat and Mass Transfer*, *151* (2020), 119359
[11] Krishna, V. M., *et al.*, Numerical Investigation of Heat Transfer and Pressure Drop for Cooling of Micro-Channel Heat Sink Using MWCNT-CuO-Water Hybrid Nanofluid with Different Mixture Ratio, *Materials Today: Proceedings*, *42* (2021), 2, pp. 969-974
[12] Bahiraei, M., *et al*., Second Law Analysis of Hybrid Nanofluid-Flow in a Micro-Channel Heat Sink Integrated with Ribs and Secondary Channels for Utilization in Miniature Thermal Devices, *Chemical Engineering and Processing-Process Intensification*, *153* (2020), 107963
[13] Hosseini, S., *et al*., Nanofluid Heat Transfer Analysis in a Micro-Channel Heat Sink (MCHS) under the Effect of Magnetic Field by Means of KKL Model, *Powder Technology*, *324* (2018), Jan., pp. 36-47
[14] Azizi, Z., *et al*., Convective Heat Transfer of Cu-Water Nanofluid in a Cylindrical Micro-Channel Heat Sink, *Energy Conversion and Management*, *101* (2015), Sept., pp. 515-524
[15] Khosravi, R., *et al*., Predicting Entropy Generation of a Hybrid Nanofluid Containing Graphene-Platinum Nanoparticles through a Micro-Channel Liquid Block Using Neural Networks, *International Communications in Heat and Mass Transfer*, *109* (2019), 104351
[16] Deng, S., *et al*., Heat Transfer and Entropy Generation in Two Layered Electroosmotic Flow of Power-Law Nanofluids through a Microtube, *Applied Thermal Engineering*, *196* (2021), 117314
[17] Azam, M., *et al*., Numerical Simulation for Variable Thermal Properties and Heat Source/Sink in Flow of Cross Nanofluid over a Moving Cylinder, *International Communications in Heat and Mass Transfer*, *118 (*2020), 104832
[18] Duangthongsuk, W., Wongwises, S., An Experimental Investigation on the Heat Transfer and Pressure Drop Characteristics of Nanofluid-Flowing in Micro-Channel Heat Sink with Multiple Zigzag Flow Channel Structures, *Experimental Thermal and Fluid Science*, *87* (2017), Oct., pp. 30-39
[19] Tripathi, D., *et al*., Joule Heating and Buoyancy Effects in Electro-Osmotic Peristaltic Transport of Aqueous Nanofluids through a Micro-Channel with Complex Wave Propagation, *Advanced Powder Technology*, *29* (2018), 3, pp. 639-653
[20] Saravani, M. S., Kalteh, M., Heat Transfer Investigation of Combined Electroosmotic/Pressure Driven Nanofluid-Flow in a Micro-Channel: Effect of Heterogeneous Surface Potential and Slip Boundary Condition, *European Journal of Mechanics-B/Fluids*, *80* (2020), Mar.-Apr., pp. 13-25
[21] Nojoomizadeh, M., *et al*., Investigation of Permeability Effect on Slip Velocity and Temperature Jump Boundary Conditions for FMWNT/Water Nanofluid-Flow and Heat Transfer Inside a Micro-Channel Filled by a Porous Media, *Physica E: Low-dimensional Systems and Nanostructures*, *97* (2018), Mar., pp. 226-238
[22] Nojoomizadeh, M., *et al.,* Investigation of Permeability and Porosity Effects on the Slip Velocity and Convection Heat Transfer Rate of Fe_3O_4/Water Nanofluid-Flow in a Micro-Channel While Its Lower Half Filled by a Porous Medium, *International Journal of Heat and Mass Transfer*, *119* (2018), Apr., pp. 891-906
[23] Lopez, A., *et al.*, Entropy Generation Analysis of MHD Nanofluid-Flow in a Porous Vertical Micro-Channel with Non-Linear Thermal Radiation, Slip Flow and Convective-Radiative Boundary Conditions, *International Journal of Heat and Mass Transfer*, *107* (2017), Apr., pp. 982-994
[24] Karimipour, A., *et al*., Simulation of Copper-Water Nanofluid in a Micro-Channel in Slip Flow Regime Using the Lattice Boltzmann Method, *European Journal of Mechanics-B/Fluids*, *49* (2015), Part A, pp. 89-99
[25] Zhao, Q., *et al*., Flow and Heat Transfer of Nanofluid through a Horizontal Micro-Channel with Magnetic Field and Interfacial Electrokinetic Effects, *European Journal of Mechanics-B/Fluids*, *80* (2020), Mar.-Apr., pp. 72-79
[26] Ma, Y., *et al*., Two-Phase Mixture Simulation of the Effect of Fin Arrangement on First and Second Law Performance of a Bifurcation Micro-Channels Heatsink Operated with Biologically Prepared Water-Ag Nanofluid, *International Communications in Heat and Mass Transfer*, *114* (2020), 104554
[27] Zhang, B., *et al*., Topology Optimization Design of Nanofluid-Cooled Micro-Channel Heat Sink with Temperature-Dependent Fluid Properties, *Applied Thermal Engineering*, *176* (2020), 115354
[28] Huminic, G., Huminic, A., Entropy Generation of Nanofluid and Hybrid Nanofluid-Flow in Thermal Systems: *A Review, Journal of Molecular Liquids*, *302* (2020), 112533

[29] Javadpour, S. M., *et al*., Optimization of Geometry and Nanofluid Properties on Micro-Channel Performance Using Taguchi Method and Genetic Algorithm, *International Communications in Heat and Mass Transfer*, *119* (2020), 104952
[30] Tanveer, A., *et al*., Theoretical Analysis of Non-Newtonian Blood Flow in a Micro-Channel, *Computer Methods and Programs in Biomedicine*, *191* (2020), 105280
[31] Ajeel, R. K., *et al*., Analysis of Thermal-Hydraulic Performance and Flow Structures of Nanofluids Across Various Corrugated Channels: An Experimental and Numerical Study, *Thermal Science and Engineering Progress*, *19* (2020), 100604
[32] Dehkordi, R.B., *et al*., Molecular Dynamics Simulation of Ferro-Nanofluid-Flow in a Micro-Channel in the Presence of External Electric Field: Effects of Fe_3O_4 Nanoparticles, *International Communications in Heat and Mass Transfer*, *116* (2020), 104653
[33] Ahmed, S., Xu, H., Forced Convection with Unsteady Pulsating Flow of a Hybrid Nanofluid in a Micro-Channel in the Presence of EDL, Magnetic and Thermal Radiation Effects, *International Communications in Heat and Mass Transfer*, *120* (2021), 105042
[34] Elbadawy, I., Fayed, M., Reliability of Al_2O_3 Nanofluid Concentration on the Heat Transfer Augmentation and Resizing for Single and Double Stack Micro-Channels, *Alexandria Engineering Journal*, *59* (2020), 3, pp. 1771-1785
[35] Karimipour, A., New Correlation for Nusselt Number of Nanofluid with $Ag/Al_2O_3/Cu$ Nanoparticles in a Micro-Channel Considering Slip Velocity and Temperature Jump by Using Lattice Boltzmann Method, *International Journal of Thermal Sciences*, *91* (2015), May, pp. 146-156
[36] Sheikhalipour, T., Abbassi, A., Numerical Analysis of Nanofluid-Flow Inside a Trapezoidal Micro-Channel Using Different Approaches, *Advanced Powder Technology*, *29* (2018), 7, pp. 1749-1757
[37] Bowers, J., *et al*., Flow and Heat Transfer Behaviour of Nanofluids in Micro-Channels, Progress in Natural Science: *Materials International*, *28* (2018), 2, pp. 225-234
[38] Elias, M., *et al*., Effect of Different Nanoparticle Shapes on Shell and Tube Heat Exchanger Using Different Baffle Angles and Operated with Nanofluid, *International Journal of Heat and Mass Transfer*, *70* (2014), Mar., pp. 289-297
[39] Huminic, G., Huminic, A., Heat Transfer and Entropy Generation Analyses of Nanofluids in Helically Coiled Tube-in-Tube Heat Exchangers, *International Communications in Heat and Mass Transfer*, *71* (2016), Feb., pp. 118-125
[40] Brinkman, H. C., The Viscosity of Concentrated Suspensions and Solutions, *The Journal of Chemical Physics*, *20* (1952), 4, pp. 571-571
[41] Yu, W., Choi, *S*., The Role of Interfacial Layers in the Enhanced Thermal Conductivity of Nanofluids: A Renovated Maxwell Model, *Journal of Nanoparticle Research*, *5* (2003), 1, pp. 167-171
[42] Xuan, Y., Roetzel, W., Conceptions for Heat Transfer Correlation of Nanofluids, *International Journal of Heat and Mass Transfer*, *43* (2000), 19, pp. 3701-3707

Paper submitted: June 1, 2021
Paper revised: October 24, 2021
Paper accepted: May 10, 2022